

Breaking the Mass Inclination Degeneracy of Radial Velocity Measurements via Monitoring von Zeipel-Lidov-Kozai Cycles: Implications in the HD 41004 System

ZHIZHEN QIN (秦至臻)^{1,2}, SHANG-FEI LIU (刘尚飞)^{1,2}, BO MA (马波)^{1,2} AND FABO FENG (冯发波)^{3,4}

¹*School of Physics and Astronomy, Sun Yat-sen University, Zhuhai 519082, China*

²*CSST Science Center for the Guangdong-HongKong-Macau Great Bay Area, Sun Yat-sen University, Zhuhai 519082, China*

³*Tsung-Dao Lee Institute, Shanghai Jiao Tong University, Shengrong Road 520, Shanghai 201210, China*

⁴*School of Physics and Astronomy, Shanghai Jiao Tong University, 800 Dongchuan Road, Shanghai 200240, China*

ABSTRACT

We investigate the dynamical stability of the S-type planet in the compact binary HD 41004. Using N -body simulations, we find that the planet could be dynamically stable at a mutual angle inclination up to $\sim 75^\circ$. The von Zeipel-Lidov-Kozai (vZLK) mechanism becomes active when the mutual inclination is greater than 39.2° . High-inclination orbits exhibit coupled oscillations in eccentricity and inclination, along with apsidal precession. Synthetic radial velocity (RV) modeling shows that these secular variations produce measurable signatures across a broad range of timescales, from full vZLK cycles to observationally accessible decades. For instance, a high mutual inclination at 75° can induce RV drifts exceeding 5 m s^{-1} per planetary orbit ($\sim 1.9 \text{ m s}^{-1} \text{ yr}^{-1}$) in circular binary configurations. The presence of eccentric vZLK further accelerates these drifts, enhancing the detectability. Long-term RV observations of this system offer a unique pathway to dynamically constrain the orbital inclination and thus determine the true mass of HD 41004 Ab. The degeneracy of mass inclination is well known when using RV measurements alone. Our results highlight that HD 41004 Ab and potentially other S-type planets in compact binaries are promising targets for breaking such a degeneracy by studying the dynamics induced by the vZLK mechanism through long-term high-precision RV monitoring.

1. INTRODUCTION

Although a significant fraction of stars are expected to reside in binary systems (Duquennoy & Mayor 1991a), the number of planets discovered in such systems remains relatively small. This disparity reflects both the observational limitations and the dynamical evolution inherent in binary environments (Musielak et al. 2005; Su et al. 2021; Stevenson et al. 2023). As of March 2025, just over 200 planets have been identified in more than 150 binary systems¹. More than half of these exoplanets are detected through radial velocity (RV) surveys (Su et al. 2021), complemented by transit photometry and high-contrast direct imaging.

Planetary orbits in binaries are generally classified as either S-type, where the planet orbits one of the two stars, or P-type, where the planet orbits the binary pair (Dvorak et al. 2002). The majority of confirmed planets in such systems are S-type, including well-studied cases

like γ Cephei Ab (Campbell et al. 1988; Hatzes et al. 2003).

However, RV method detects periodic velocity changes of a star along the observer's line of sight, i.e. the amplitude of perturbations is proportional to the minimum mass of a planet. The true mass of the planet and its orbital inclination (relative to the sky plane) are degenerate parameters via the RV measurement alone, which are crucial to characterize hierarchical systems. Recent efforts have aimed to overcome these limitations. For instance, Stevenson et al. (2023) proposed improved strategies for detecting S-type planets, while Chauvin et al. (2023) employed a combination of RV measurements, speckle interferometry, high-contrast imaging, and astrometry to revisit the dynamically complex HD 196885 system. In addition, Huang et al. (2025) utilized dynamical RV fitting to better constrain the orbital parameters of S-type planets in close binaries.

The dynamical architectures of binary planetary systems offer critical insights into planet formation and long-term evolution (Heppenheimer 1978; Haghighipour 2006; Xie et al. 2010; Gong & Ji 2018; Fragione 2018; Camargo et al. 2023). Notably, Su et al. (2021) finds that

liushangfei@mail.sysu.edu.cn

¹ <https://adg.univie.ac.at/schwarz/multiple.html>

S-type planets in binaries typically exhibit higher orbital eccentricities than those around single stars. Close binaries, in particular, appear to host a distinct population of massive, short-period planets, suggesting unique dynamical histories (Zucker & Mazeh 2002; Su et al. 2021).

The complex dynamical architectures of binary systems have motivated extensive theoretical and numerical studies on planetary stability and habitability. Pioneering work by Holman & Wiegert (1999) establishes an empirical expression for the critical semi-major axis beyond which planetary orbits become unstable. Subsequent studies employ different methods from direct integration to chaos indicators such as the Fast Lyapunov Indicator (FLI; Benettin et al. 1980; Froeschlé et al. 1997) and MEGNO (Cincotta, P. M. & Simó, C. 2000) to explore the role of mutual inclination, eccentricity, and orbital spacing in shaping long-term stability (Pilat-Lohinger & Dvorak 2002; Dvorak et al. 2002; Szenkovits & Makó 2008; Pilat-Lohinger et al. 2003; Satyal et al. 2013; Satyal et al. 2014; Quarles et al. 2020; Tory et al. 2022; Bhaskar & Perets 2024). For instance, Dvorak et al. (2002) shows that moderate inclinations ($\lesssim 50^\circ$) can enlarge the stability region, while Szenkovits & Makó (2008) and Satyal et al. (2013) systematically mapped the stability boundaries using Hill criteria (Hill 1878; Makó & Szenkovits 2004) and chaos diagnostics. The stability of inclined orbits in binary-planet and multi-planet systems has also been extensively investigated (Pilat-Lohinger et al. 2003; Quarles et al. 2020; Tory et al. 2022; Veras & Armitage 2004; Bhaskar & Perets 2024).

The stability results discussed above highlight the critical role of mutual inclination in shaping the dynamical evolution of planetary systems in compact binaries. Beyond determining orbital stability, mutual inclination also governs the onset of long-term secular interactions. In hierarchical triple systems, the dominant mechanism responsible for such interactions is the von Zeipel-Lidov-Kozai (vZLK) mechanism (von Zeipel 1910; Lidov 1962; Kozai 1962). This mechanism drives long-term oscillations in eccentricity and inclination, accompanied by apsidal and nodal precession, under the influence of a distant, inclined companion. Originally developed to describe asteroid dynamics perturbed by Jupiter, the vZLK mechanism is most effective for mutual inclinations between 39.2° and 140.8° , and has since been extended to a wide range of astrophysical contexts (Harrington 1968; Wu & Murray 2003; Ford et al. 2004; Fabrycky & Tremaine 2007; Teyssandier et al. 2013; Naoz et al. 2013; Ito & Ohtsuka 2019). In compact binaries such as γ Cephei (Heintz 1982; Pourbaix et al. 1999; Pourbaix & Boffin 2016), the eccentric vZLK extension

has been used to account for the influence of nonzero eccentricities in both the inner and outer orbits (Lithwick & Naoz 2011; Li et al. 2014; Naoz 2016; Huang & Ji 2022). The same mechanism may have reshaped the stability landscape of some other compact binary systems, such as HD 196885 and α Centauri (Satyal et al. 2014; Quarles & Lissauer 2016; Giuppone & Correia 2017).

However, most of these studies focus on the stability of vZLK dynamics. Thus, it is natural to ask whether such secular effects could manifest in real planetary systems—and under what conditions they become observable. Among compact binaries, HD 41004 stands out as a particularly compelling case for studying vZLK-induced dynamics due to its tight configuration and massive stellar companion. Discovered via the pioneering application of multi-order TODCOR to echelle spectra (Zucker & Mazeh 1994; Santos et al. 2002; Zucker, S. et al. 2003), HD 41004 is a hierarchical four-body system consisting of a primary K0V star (HD 41004 A), its planetary companion (HD 41004 Ab), and a close binary companion (HD 41004 B + Bb), composed of an M2V star and a brown dwarf (see Table 1). The planet orbits at 1.7 AU, while the secondary binary lies at a projected distance of ~ 22 AU, enabling strong secular perturbations. The system’s complexity has prompted advanced modeling efforts; for instance, Andrade-Ines et al. (2016) emphasizes the need for second-order perturbation theory (Laskar & Boué 2010), and Satyal & Musielak (2016) identifies a critical inclination near 65° for dynamical stability. Despite its dynamical richness, previous observations place only weak constraints on the system parameters, and the long-term secular evolution of HD 41004—particularly in the high mutual inclination regime—remains poorly understood.

If the mutual inclination between the planetary and binary orbits exceeds the vZLK threshold, the system may exhibit long-term orbital variations, including eccentricity and inclination oscillation, and secular precession—potentially detectable via RV monitoring, transit timing variations, or high-precision astrometry.

In this study, we investigate the dynamical stability of the HD 41004 system and explore the long-term observational signatures in radial velocity associated with vZLK cycles. By combining theoretical modeling, numerical simulations, and dynamical analysis, we aim to clarify the conditions under which vZLK effects are triggered and to identify potential observational diagnostics. The theoretical framework, governing equations, and simulation setup are detailed in Section 2. Simulation results are presented in Section 3, followed by a discussion in Section 4, and a summary of key findings in Section 5.

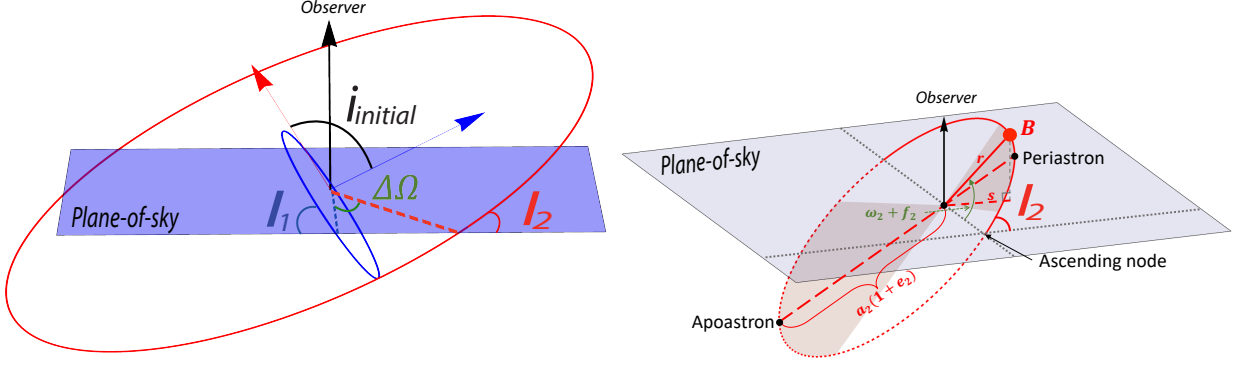


Figure 1. Schematic geometry of a hierarchical three-body system and projected separation s of HD 41004 B. Left panel: the blue plane represents the plane of the sky, perpendicular to the observer’s line of sight (black arrow). Red and blue arrows denote the orbital angular momentum vectors of the outer and inner orbits, respectively. The angles I_1 and I_2 are their inclinations relative to the plane of the sky, while i_{initial} is the mutual inclination between the two orbits. The green angle $\Delta\Omega$ represents the difference in the longitudes of ascending nodes. Although I_1 and I_2 depend on the observer’s orientation, both i_{initial} and $\Delta\Omega$ are intrinsic dynamical parameters of the system. Right panel: the red ellipse shows a representative orbit of component B with eccentricity e_2 and inclination I_2 . The gray sectors illustrate orbital phase angle $\omega_2 + f_2$ within $\pm 60^\circ$ around periastron and apoastron. The projected separation s , instantaneous distance r , and inferred semi-major axis a_2 follow the definitions in Equation 3.

2. METHODS

2.1. Orbital Configuration and Parameter Setup of HD 41004

In hierarchical triple systems, the orbital configuration can be described by two nested orbits: an inner orbit between a central body m_0 and an inner companion m_1 , and an outer orbit between the center of mass of the inner pair and an external perturber m_2 . Each orbit is characterized by its semi-major axis, eccentricity, inclination relative to a chosen reference plane (commonly the plane of the sky), and orientation angles (longitude of ascending node Ω and argument of periastron ω).

The mutual inclination i_{initial} between the inner and outer orbits is a key parameter governing secular interactions, including the vZLK mechanism. This inclination is defined as the angle between the orbital angular momentum vectors of the inner and outer orbits and is related to the observable orbital inclinations I_1 , I_2 and the nodal difference $\Delta\Omega$ via:

$$\cos i_{\text{initial}} = \cos I_1 \cos I_2 + \sin I_1 \sin I_2 \cos \Delta\Omega. \quad (1)$$

While I_1 and I_2 are orientation-dependent quantities tied to the observer’s line of sight, i_{initial} is an intrinsic property of the system’s dynamical configuration and remains invariant under changes in viewing geometry (see the left panel of Figure 1).

In the context of radial velocity (RV) observations, the true masses of orbiting companions are not directly measured; instead, only the minimum masses $m_1 \sin I_1$ and $m_2 \sin I_2$ are inferred. These are given by (Lee & Peale 2003):

$$K_1 = \left(\frac{2\pi G}{P_1} \right)^{1/3} \frac{m_1 \sin I_1}{(m_0 + m_1)^{2/3}} \frac{1}{\sqrt{1 - e_1^2}}; \\ K_2 = \left(\frac{2\pi G}{P_2} \right)^{1/3} \frac{m_2 \sin I_2}{(m_0 + m_1 + m_2)^{2/3}} \frac{1}{\sqrt{1 - e_2^2}}. \quad (2)$$

This mass-inclination degeneracy is critical for the dynamical evolution of the system, as different combinations of inclination, true mass, and eccentricity can produce the same RV signals but lead to different orbital paths and dynamical outcomes.

Following Hamers & Lai (2017), we treat the quadruple HD 41004 system as a hierarchical three-body configuration, approximating HD41004 B+Bb as a single component B, to facilitate the analysis of the long-term orbital evolution of planet Ab. m_0 , m_1 , and m_2 thus denote masses of the primary star HD 41004 A, the S-type planetary companion HD 41004 Ab, and the compact companion HD 41004 B+Bb, respectively. The complete list of observational and simulation parameters adopted in this study is summarized in Table 1.

The observational inclination (I_1) of planet Ab is derived from the binary inclination (I_2) and the mutual inclination (i_{initial}) using Equation 1. In our stability simulations, we adopt a minimum mass of $m_1 \sin I_1 = 2.54 M_J$ reported by Zucker, S. et al. (2004).

The orbit of HD 41004 B remains poorly constrained. The sky-projected separation (s) of the stellar binary is approximately 22 AU (Zucker, S. et al. 2003, 2004). However, the true semi-major axis (a_2) may differ sub-

Table 1. Parameters of the HD 41004 system constrained by observations and explored in our dynamical modeling

Parameter	Observation ^a	Stability Simulations	RV Simulations
HD 41004 A			
Mass (m_0)	$0.7 M_\odot$	$0.7 M_\odot$	$0.7 M_\odot$
HD 41004 Ab			
Minimum mass ($m_1 \sin I_1$)	$(2.54 \pm 0.74) M_J$	$2.54 M_J$	$1.8, 2.54, 3.28 M_J$
RV Semi-amplitude (K_1)	$99 \pm 60 \text{ m s}^{-1}$	—	—
Semi-major Axis (a_1)	$1.7 \pm 0.04 \text{ AU}$	1.7 AU	1.7 AU
Eccentricity (e_1)	0.74 ± 0.2	0.74	0.74
Argument of Pericenter (ω_1)	$97^\circ \pm 31^\circ$	97°	97°
Line-of-sight Inclination (I_1)	—	determined via Eq. (1)	determined via Eq. (1)
Mutual Inclination (i_{initial})	—	$[0^\circ, 90^\circ]$	$0^\circ, 30^\circ, 45^\circ, 60^\circ, 75^\circ$
HD 41004 B+Bb			
Mass (m_2)	$0.40 + 0.02 M_\odot$	$0.40 + 0.02 M_\odot$	$0.40 + 0.02 M_\odot$
Semi-major Axis (a_2)	$\sim 22 \text{ AU}$	$[12.2, 220.0]^\text{b} \text{ AU}$	$22, 25, 30, 40 \text{ AU}$
Eccentricity (e_2)	—	$0, 0.4, 0.8$	$0, 0.4$
Line-of-sight Inclination (I_2)	—	$0^\circ, 45^\circ, 90^\circ$	90°
Nodal Difference ($\Delta\Omega$)	—	$[0^\circ, 360^\circ]^\text{c}$	$[0^\circ, 360^\circ]^\text{c}$

NOTE— Square brackets [] denote variable parameter ranges, while comma-separated values indicate fixed values in the simulations. Unspecified orbital parameters are assumed to be zero.

^a Observation parameters from Santos et al. (2002); Zucker, S. et al. (2003, 2004). a_2 denotes the projected binary separation (21-23 AU), not the true semi-major axis. ^b The specific parameter combinations for a_2 in the stability simulations are listed in Table 2. ^c In the simulations, the initial nodal difference $\Delta\Omega = \Omega_1 - \Omega_2$ is set to 0° and evolves dynamically over the range $[0^\circ, 360^\circ]$.

stantially from s , depending on the inclination (I_2), orbital phase angle ($\omega_2 + f_2$), and eccentricity (e_2) (see the right panel of Figure 1). The value of a_2 can be estimated using Kepler’s laws (Greco & Burrows 2015):

$$\begin{aligned}
 a_2 &= \frac{r}{1 - e_2^2} (1 + e_2 \cos f_2) \\
 &= \frac{s}{(1 \pm e_2) \sin \theta} \\
 &= \frac{s}{(1 \pm e_2) \sqrt{1 - \sin^2 I_2 \sin^2(\omega_2 + f_2)}}.
 \end{aligned} \tag{3}$$

To study the dynamical influences of HD 41004 B, we explore a range of a_2 in our stability analysis by varying I_2 and e_2 . We adopt $e_2 = 0, 0.4, 0.8$, reflecting the typical eccentricities of stellar binaries (Duquennoy & Mayor 1991b). Taking the assumption that component B has an orbital phase angle $\omega_2 + f_2$ within $\pm 60^\circ$ around either periastron or apoastron (the gray sectors in the right panel of Figure 1), a_2 spans a broad range between different I_2 (see Equation 3) except for the trivial configuration in which $e_2 = 0$, $I_2 = 0^\circ$ and thus $a_2 \equiv 22 \text{ AU}$, as summarized in Table 2. Such a choice covers $\sim 67 - 91\%$ of the orbital period for e_2 from 0 to 0.8, and includes both the minimum and maximum

semi-major axes consistent with the projected separation.

Table 2. Suite of orbital parameters of the stellar binary HD 41004 B for the stability analysis of HD 41004 Ab.

e_2	I_2 (deg)	a_2 Range (AU)
0	0°	22.0
	45°	22.0 – 31.1
	90°	22.0 – 44.0
0.4	0°	15.7 – 36.7
	45°	15.7 – 51.9
	90°	15.7 – 73.3
0.8	0°	12.2 – 110.0
	45°	12.2 – 155.6
	90°	12.2 – 220.0

For RV simulations including dynamical fitting of existing RV data and observational signatures of RV drifts (the third column of Table 1), we simply fix I_2 , as we shall show that the impact of I_2 is not significant on a relatively short timescale. However, changes in a_2 and e_2 can substantially alter RV signals on one planetary orbit.

2.2. *N*-body Dynamical Modeling

To explore the dynamical stability and potential observational signatures in radial velocity measurements of the HD 41004 system, we perform numerical simulations using the `rebound` *N*-body integrator (Rein & Liu 2012; Rein & Spiegel 2015). Our study focuses on three main objectives: (1) mapping the system’s stability across a range of orbital configurations; (2) performing unrestricted three-body dynamical modeling to fit the existing RV data; and (3) generating synthetic high-precision RV datasets to investigate the potential observational signatures of vZLK cycles acting on planet Ab.

2.2.1. Stability Analysis

Earlier work (e.g., Satyal & Musielak 2016; Giuppone & Correia 2017) approximates the HD 41004 system using a three-dimensional elliptic restricted three-body problem (ER3BP) approximation, in which HD 41004 B and its brown dwarf companion are treated as a single perturbing mass, while planet Ab is modeled as a massless test particle.

In this study, we model the system with unrestricted three-body dynamics and assess its stability using the Mean Exponential Growth Factor of Nearby Orbits (MEGNO) indicator (see Appendix A), which can efficiently distinguish between stable, quasi-periodic (with $\bar{Y} \rightarrow 2$) and chaotic orbits (where \bar{Y} diverges). This approach allows us to effectively map dynamical regimes and identify instability boundaries within a vast parameter space.

Because the planetary mass has the least impact on the dynamical stability except for the plane-of-sky case ($I_1 = 0^\circ$), in our unrestricted hierarchical three-body model, the minimum mass of the planet $m_1 \sin I_1$ is fixed ignoring its uncertainty, while I_2 and e_2 are allowed to vary to explore the parameter space of mutual inclinations (i_{initial}) and binary separations (a_2). The planetary inclination I_1 is adjusted via Equation (1) to account for the mass-inclination degeneracy (Stevenson et al. 2023). For simplicity, we set $\Delta\Omega = 0$ and adopt three representative values of I_2 (0° , 45° , 90°). We run simulations on a uniform 50×50 grid in a_2 - i_{initial} space and each one is integrated over 2×10^6 planetary orbits. The relevant parameters are summarized in Tables 1 and 2.

We perform high-precision integrations using the IAS15 integrator and construct MEGNO maps to identify stable and unstable regions. Also, orbits were deemed unstable if the vZLK mechanism induced strong eccentricity growth, causing the pericenter to fall below the Roche limit. The combined use of MEGNO and the

Roche limit criterion offers a reliable approach to assess long-term dynamical stability. We show the results in Section 3.1.

2.2.2. RV Simulations

On the timescale of the observation of HD 41004 A, planetary effects dominate the RV variations of the primary star. Zucker, S. et al. (2003, 2004) derive a minimum mass $m_1 \sin I_1$ of $2.54 \pm 0.74 M_J$ with a Keplerian fit ignoring its stellar companion. However, to extract potential vZLK cycles from long-term RV signals, the binary effects must be taken into account.

We first simulate the unrestricted three-body system and generate the synthetic RV signals of HD 41004 A, accounting for gravitational perturbations from HD 41004 Ab and B. The simulated RV signals are then compared with the observational data to evaluate the impacts of varying a_2 , e_2 , i_{initial} and $m_1 \sin I_1$ (Table 1). For each configuration, we perform a phase search that spans at least a full orbit of companion B to find the best fit. The RV fitting results are presented in Section 3.2.

We further synthesize long-term RV variations of HD 41004 A due to its planetary and stellar companions in configurations that are stable and consistent with RV observations. To identify potential vZLK oscillations in RV signatures, we perform a two-step procedure to isolate the planetary component: (1) integrating the full three-body system to obtain the total RV signal of HD 41004 A, and (2) subtracting the modeled binary-induced contribution. The results of long-term RV variations in possible configurations are summarized in Section 3.3

3. RESULTS

3.1. Stability of the HD 41004 System

The empirical stability criterion developed by Holman & Wiegert (1999) and refined by Ballantyne et al. (2021) provides a practical baseline for evaluating the stability of S-type planetary orbits in binary systems. The critical semi-major axis a_{critical} , beyond which planetary orbits are expected to become unstable, is given by:

$$a_{\text{critical}} = a_2(0.464 - 0.380\mu - 0.631e_2 + 0.586\mu e_2 + 0.150e_2^2 - 0.198\mu e_2^2), \quad (4)$$

where a_2 is the binary semi-major axis, e_2 the binary eccentricity, and $\mu = m_2/(m_0 + m_2)$ the binary mass ratio. For the HD 41004 system, adopting $a_2 = 22$ AU and $\mu \approx 0.375$, the critical semi-major axes are $a_{\text{critical}} \approx 7.07$ AU, 3.72 AU, and 0.90 AU for $e_2 = 0$, 0.4, and 0.8, respectively. The planet HD 41004 Ab, with $a_1 = 1.7$ AU, lies well within the stability threshold for low to moderate binary eccentricities.

However, this criterion may not be legitimate if the mutual inclination is high. Secular perturbations such as the vZLK mechanism are not considered either. [Satyal & Musielak \(2016\)](#) has identified a stability threshold at a mutual inclination near 65° in the HD 41004 system based on the Hill Stability Function. But the analysis is limited by the test-particle approximation adopted for the planet. Besides, parameters in their study also differ from those in [Zucker, S. et al. \(2004\)](#), which may affect their stability results.

In figure 2 we plot the MEGNO stability maps of eight non-trivial configurations (see Table 2. The configuration of $e_2 = 0$ and $I_2 = 0$ is excluded, because the binary orbit is fixed by geometry). The horizontal axis in each panel indicates the binary semi-major axis a_2 confined by orbital configurations. The left vertical axis of each panel denotes the initial mutual inclination i_{initial} , which determines the planetary inclination I_1 and the true mass m_1 (right vertical axis) by Equation 1 and the observed minimum mass. The solid red line marks the critical inclination of 39.2° for the onset of the vZLK oscillations, while the dashed line at 75° denotes the approximate instability threshold.

The stability maps suggest that whether a hierarchical system is stable or not is mainly determined by its mutual inclination (i_{initial}) and perturbations from the stellar companion. In the first row of Figure 2, when the binary orbit is circular ($e_2 = 0$), HD 41004 Ab remains stable up to $i_{\text{initial}} \sim 75^\circ$ for the entire range of a_2 . In the second row, when the binary orbit has a mild eccentricity ($e_2 = 0.4$), the planet becomes unstable due to enhanced gravitational perturbations near the binary’s periastron, where the reduced separation $a_2(1 - e_2)$ undermines stability. In addition, planetary orbits are unstable at the mutual inclination close to the onset of the vZLK effect, $i_{\text{initial}} = 39.2^\circ$. This unstable region arises from vZLK-induced eccentricity and inclination oscillations, with ω_1 circulating (0° - 360°) rather than librating around 90° , thus preventing resonant locking and leading to long-term instability. This is consistent with previous findings ([Satyal et al. 2014](#); [Giuppone & Correia 2017](#)), i.e. high a_1/a_2 ratios and mutual inclinations around 39.2° as well as extreme mutual inclinations could trigger instability. Note that the planet could be very massive when $I_2 = 0^\circ$ and $i_{\text{initial}} \sim 0$. However, the likelihood is rather remote. Highly eccentric cases ($e_2 = 0.8$) in the bottom row further demonstrate that maintaining long-term stability requires even larger binary separation a_2 .

To summarize, numerical simulations reveal a persistent stability limit at $i_{\text{initial}} \sim 75^\circ$, which remains robust

across variations in planet Ab’s true mass and observational inclination.

3.2. Dynamical Fitting of Existing RV data

To constrain the orbital architecture of HD 41004, we perform unrestricted three-body simulations to fit the RV observations. Figure 3 displays two representative cases with fixed parameters $m_1 \sin I_1 = 2.54 M_J$ and $a_2 = 22$ AU: (a) varying e_2 at $i_{\text{initial}} = 0^\circ$ (top panel), and (b) varying i_{initial} at $e_2 = 0$ (bottom panel). In each panel, we plot the combined RV signals of Ab and B, the isolated planetary contribution after binary signal subtraction, and the observed-minus-calculated (O-C) residuals, respectively. Distinct colors and line styles denote various configurations, while data points with error bars are RV observational data, and the systemic velocity of 42.513 km s^{-1} is subtracted for consistency ([Zucker, S. et al. 2004](#)). The root-mean-square (RMS) values for each model are indicated in the legends, with the time axis referenced to JD 2451902.77432, the epoch of the first RV measurement.

In the top panel of Figure 3, configurations with $e_2 = 0$ and $e_2 = 0.4$ achieve RMS residuals of $\sim 10 \text{ m s}^{-1}$, consistent with the Keplerian fit reported by [Zucker, S. et al. \(2004\)](#). For $e_2 \geq 0.5$, the RMS values increase by $\geq 25\%$, indicating significantly degraded fits. These optimal fits correspond to specific orbital phases of companion B, which induce phase shifts in planet Ab’s orbit and drive distinct RV evolutionary patterns across eccentricity regimes.

In the bottom panel of Figure 3, fitting accuracy remains consistent with observations across all i_{initial} values, with optimal fits corresponding to specific orbital phases of companion B. These phase-dependent configurations induce offsets in planet Ab’s RV signal, thereby generating distinct evolutionary patterns in the combined RV curve of component A.

We extend the analysis to broader parameter spaces—including a_2 and $m_1 \sin I_1$ —with detailed results in Appendix B. Dynamical fits for wide binaries ($a_2 > 22$ AU) with eccentricities $e_2 \lesssim 0.5$ consistently yield RMS residuals of $\sim 10 \text{ m s}^{-1}$, aligning with the observational precision. While extreme values of the minimum planet mass ($m_1 \sin I_1$)—whether significantly larger or smaller than the nominal $2.54 M_J$ —systematically degrade the fitting quality, as evidenced by elevated RMS residuals.

In summary, our unrestricted three-body fits constrain the HD 41004 binary to a low-to-moderate eccentricity regime ($e_2 \lesssim 0.5$) and yield a minimum planetary mass $m_1 \sin I_1 \sim 2.54 M_J$. However, degeneracies prevent tight constraints on the binary separation a_2 and initial

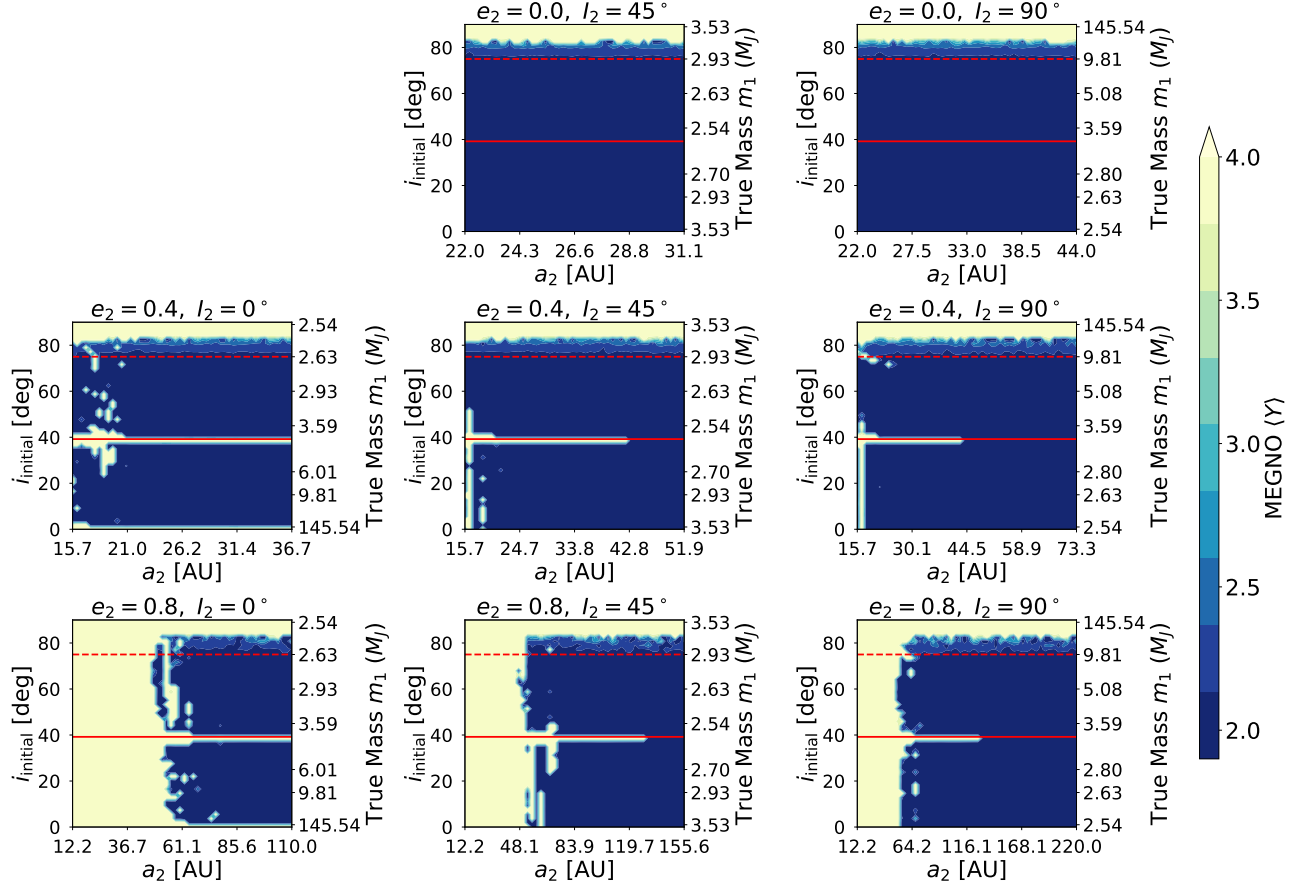


Figure 2. MEGNO stability maps for the HD 41004 system under varying binary eccentricities and observational inclinations. Each panel depicts the dynamical stability of planet Ab for specific combinations of binary eccentricity (e_2) and inclination (I_2). The x -axis represents the binary semi-major axis a_2 , and the left y -axis shows the mutual inclination i_{initial} . The right y -axis displays the true mass m_1 inferred from $m_1 \sin I_1 = 2.54 M_J$. The color shading indicates MEGNO values: blue ($\bar{Y} \simeq 2$) represents stable, quasi-periodic motion, while yellow-white ($\bar{Y} > 2$) denotes chaotic behavior. The red dashed line marks $i_{\text{initial}} = 75^\circ$, and the solid line represents the critical inclination of 39.2° for vZLK excitation. For $e_2 = 0$, stability is maintained up to 75° across all a_2 . At $e_2 = 0.4$ and $e_2 = 0.8$, instability emerges at smaller a_2 and near $i_{\text{initial}} = 39.2^\circ$ due to enhanced eccentric vZLK forcing. The top-left panel is blank, as a_2 is fixed for $I_2 = 0$ and $e_2 = 0$, making simulations unnecessary.

mutual inclination i_{initial} . These limitations underscore the necessity of future high-cadence RV observations of this system to resolve its full orbital architecture.

3.3. vZLK-induced Planetary RV Signatures

Both dynamical stability analysis and RV fitting permit HD 41004 Ab to maintain a high-inclination orbit ($i_{\text{initial}} \lesssim 75^\circ$) relative to the binary plane. When i_{initial} exceeds the critical angle of 39.2° , the vZLK mechanism activates. In compact eccentric binaries, the eccentric vZLK mechanism further amplifies and accelerates the excitation of the planet’s eccentricity and inclination.

The vZLK timescale governs the coupled oscillations of planetary inclination and eccentricity. In the test-particle approximation, the vZLK timescale follows the

analytical expression (Naoz 2016; Antognini 2015):

$$t_{\text{vZLK}} \simeq \frac{16}{15} \left(\frac{a_2^3}{a_1^{3/2}} \right) \sqrt{\frac{m_0}{Gm_2^2}} (1 - e_2^2)^{3/2}, \quad (5)$$

which yields 1.02×10^4 yr at $e_2 = 0$ and 7.89×10^3 yr at $e_2 = 0.4$ assuming $a_2 = 22$ AU for the HD 41004 system.

Beyond the test-particle approximation, the vZLK timescale exhibits significant parameter dependence (Antognini 2015; Naoz 2016; Hamers 2021). We quantify this through numerical simulations across mutual inclinations $i_{\text{initial}} \in [40^\circ, 75^\circ]$. For $a_2 = 22$ AU:

- At $e_2 = 0$: t_{vZLK} decreases from $\sim 9.0 \times 10^3$ yr to $\sim 2.3 \times 10^3$ yr
- At $e_2 = 0.4$: t_{vZLK} decreases from $\sim 4.5 \times 10^3$ yr to $\sim 1.7 \times 10^3$ yr

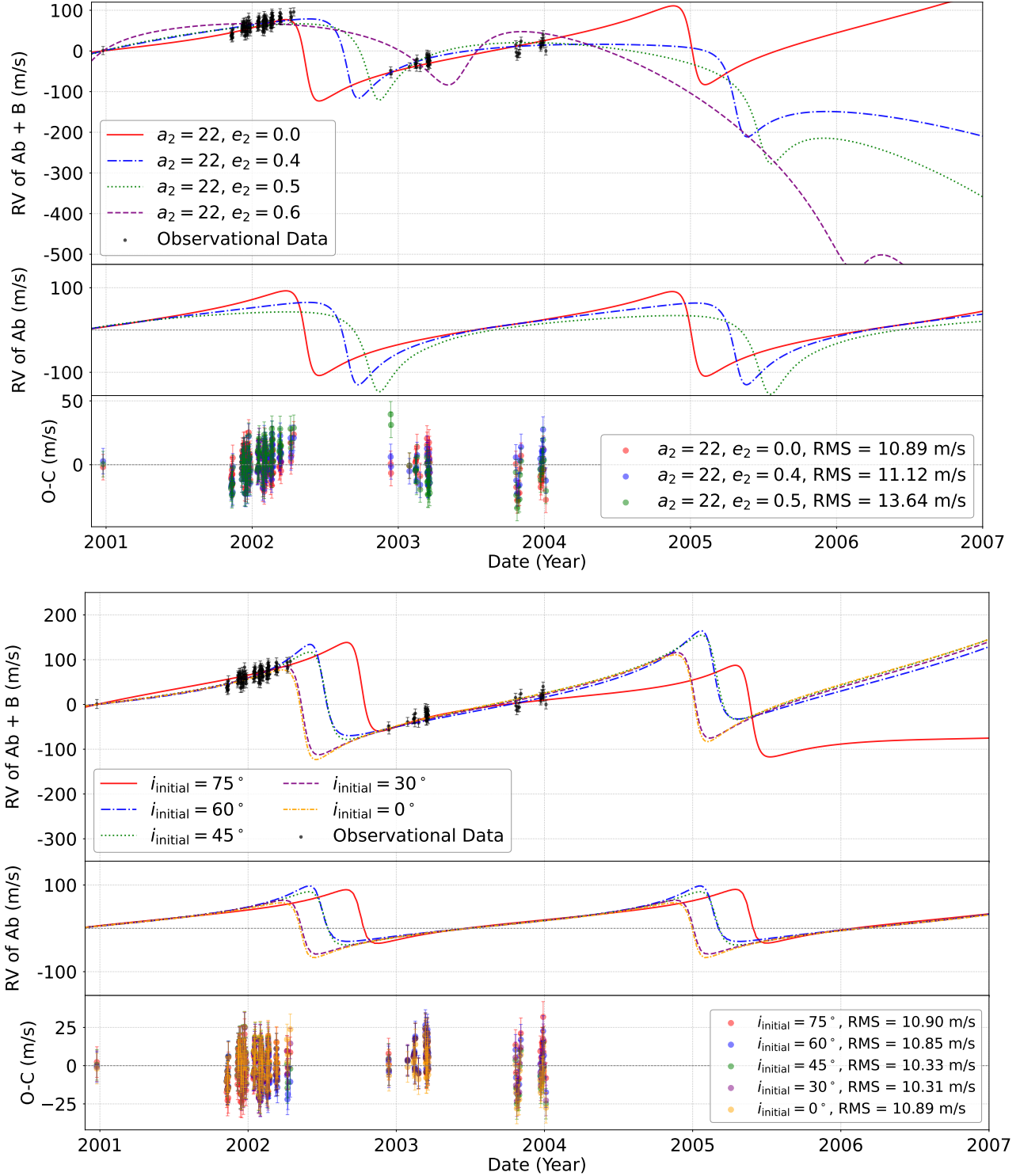


Figure 3. Dynamical RV Fitting of HD 41004 A under different orbital configurations. In each plot, the top panel displays the combined RV signal of HD 41004 A, incorporating contributions from both the planetary companion (Ab) and the stellar companion (B). The middle panel presents the isolated planetary signal after subtracting the RV contribution of companion B. The bottom panel shows the O-C (Observed minus Calculated) residuals for each fit. Different colors and line styles represent varying eccentricities of the stellar companion (e_2) or different initial mutual inclinations (i_{initial}), depending on the scenario. The top figure corresponds to $a_2 = 22$ AU with different e_2 and fixed $i_{\text{initial}} = 0^\circ$, while the bottom figure shows $a_2 = 22$ AU with $e_2 = 0$ and varying i_{initial} . The legend in each panel provides the RMS values of the O-C residuals for each configuration. Observed RV data points are plotted with error bars, and the systemic velocity of 42.513 km s^{-1} is subtracted for consistency (Zucker, S. et al. 2004). The time axis is referenced to JD 2451902.77432 (2000 December), marking the epoch of the first published RV measurement.

with increasing i_{initial} (see Appendix C for full parameter scans). Higher mutual inclinations systematically shorten vZLK cycles, accelerating planet Ab’s dynamical evolution and enhancing its detectability via time-domain signatures in RV and transit surveys.

Following the RV signal retrieval method (Section 2.2.2), we isolate the RV signals of HD 41004 Ab across initial mutual inclinations $i_{\text{initial}} \in [0^\circ, 75^\circ]$. Our simulations span 2×10^6 days (~ 5479 yr), sufficient to resolve full vZLK cycles for $i_{\text{initial}} \geq 45^\circ$.

In Figure 4 we show the simulated RV curves of HD 41004 Ab with a minimum mass $m_1 \sin I_1 = 2.54 M_J$ under distinct dynamical configurations. In panels (a) and (b) we fix $a_2 = 22$ AU and compare the results of varying initial mutual inclinations i_{initial} with a binary eccentricity of $e_2 = 0$ and $e_2 = 0.4$, respectively. Both show prominent vZLK-driven RV oscillations at $i_{\text{initial}} \geq 60^\circ$. In panels (c) and (d) we fix $i_{\text{initial}} = 75^\circ$ and compare the results of varying different binary separation a_2 with a binary eccentricity of $e_2 = 0$ and $e_2 = 0.4$, respectively. Both highlight enhanced RV variations due to large mutual inclination.

More specifically, these signatures result from the combined influence of the following effects:

1. The initially high mutual inclination (i_{initial}), which corresponds to a lower observational inclination (I_1), leads to a larger true planetary mass. This amplification enhances the RV signal as I_1 increases and eccentricity is driven up during vZLK cycles. The maximum semi-amplitude K_1 reaches nearly 750 m s^{-1} for $i_{\text{initial}} = 75^\circ$ and approximately 150 m s^{-1} for $i_{\text{initial}} = 60^\circ$, coinciding with peak I_1 and e_1 . Secular eccentricity oscillations modulate the RV curve shape, especially near periastron. In contrast, for lower mutual inclinations, K_1 remains stable around 100 m s^{-1} .
2. Apsidal precession, induced by the secular interaction, gradually shifts the orientation of the orbit. This in turn alters the symmetry of the stellar reflex motion, eventually leading to a reversal in the net RV trend—from predominantly positive to negative values.
3. When $e_2 \neq 0$, eccentric vZLK is activated, shortening the vZLK timescale. As shown in panel (b), the RV variations become more rapid compared to panel (a) across different initial inclinations.
4. Larger a_2 extends the vZLK timescale. In panel (c), the minimum planetary mass remains constant, variations in K_1 across different a_2 are minimal. However, the slower vZLK evolution leads

to more gradual RV modulations. In panel (d), increasing e_2 shortens the vZLK timescale, accelerating Ab’s orbital evolution, which is reflected in the RV curve.

Although a complete vZLK cycle—typically spanning several thousand years—is beyond the reach of the observation, its dynamical imprints can still be detected on much shorter timescales. The two panels of Figure 5 show simulated planetary RV curves over a 40-year baseline for different i_{initial} , with a fixed binary separation $a_2 = 22$ AU and a binary eccentricity of $e_2 = 0$ and $e_2 = 0.4$, respectively. At high mutual inclinations, perturbations from the binary induce a systematic drift in the planetary RV signal: $i_{\text{initial}} = 75^\circ$ leads to $\sim 5 \text{ m s}^{-1}$ per planetary orbit for $e_2 = 0$ and $\sim 10 \text{ m s}^{-1}$ for $e_2 = 0.4$, while $i_{\text{initial}} = 60^\circ$ shows approximately half of these values. This drift is most prominent near the periastron, where the high orbital velocity amplifies small perturbations. Secular precession of the periastron under vZLK gradually shifts the phase of RV maxima, contributing to the cumulative drift across orbits. In contrast, at lower inclinations, the binary’s perturbations are negligible, and the planetary RV curves remain nearly unchanged throughout the 40-year baseline.

In summary, although a full vZLK cycle spans thousands of years, its dynamical effects can manifest on much shorter timescales, particularly in systems with high mutual inclinations. In addition, eccentric vZLK effect can further accelerate these variations. Over decadal baselines, high-inclination configurations exhibit detectable deviations from near-coplanar motion, including secular RV drifts. These short-term signatures of coupled oscillations in inclination and eccentricity are most pronounced near the periastron, which can be captured by current and future high-cadence RV measurements. Systems like HD 41004 therefore serve as ideal laboratories for probing secular evolution via multi-decade RV campaigns, resolving the fundamental mass-inclination degeneracy unattainable with snapshot RV measurements.

4. DISCUSSION

4.1. Observational Prospects for Dynamical Signatures

The activation and amplitude of the vZLK oscillations are governed by mutual inclination i_{initial} , while their period and evolutionary timescales are controlled primarily by binary orbital parameters a_2 and e_2 (see Section 3.3 for detailed discussion). In general, smaller a_2 , higher e_2 , and larger i_{initial} lead to shorter modulation timescales and stronger RV drifts. For high-inclination configurations ($i_{\text{initial}} \gtrsim 60^\circ$) in compact binaries ($a_2 \lesssim 40$ AU), vZLK-induced RV deviations be-

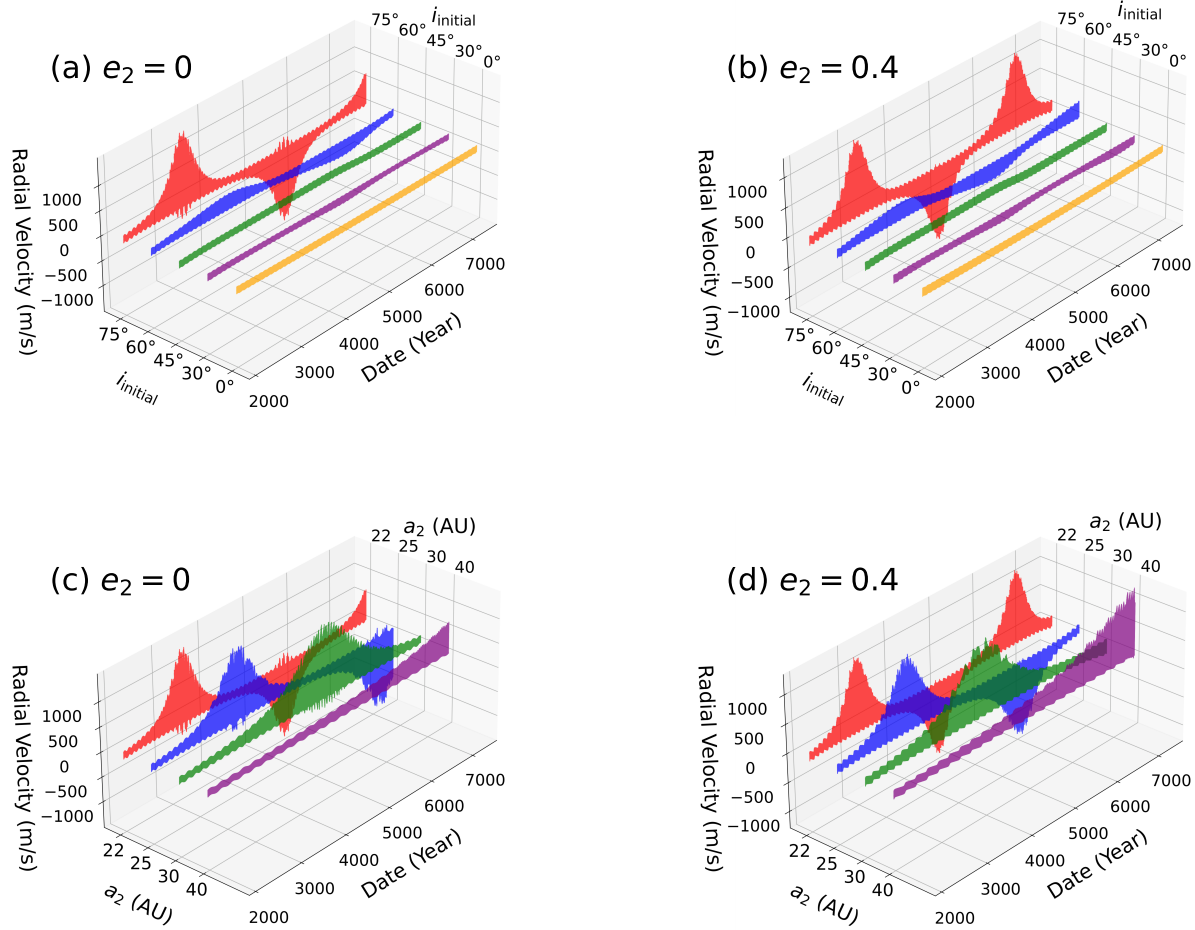


Figure 4. Simulated RV curves of HD 41004 Ab for various configurations over 2×10^6 days (~ 5479 yr). The panel (a) corresponds to $a_2 = 22$ AU, $e_2 = 0$, and $m_1 \sin I_1 = 2.54 M_J$, with varying initial mutual inclinations (i_{initial}). The panel (b) shows the same configuration except with $e_2 = 0.4$. In the panel (c), the simulation explores $a_2 = 22, 25, 30, 40$ AU, $e_2 = 0$, and $m_1 \sin I_1 = 2.54 M_J$, with $i_{\text{initial}} = 75^\circ$. The panel (d) follows the same setup as the bottom-left, but with $e_2 = 0.4$.

come detectable within 10-40 year baselines at $\geq 5\sigma$ confidence with current RV precision ($\sim 1 \text{ m s}^{-1}$).

We note that the reported minimum mass of planet Ab carries a significant uncertainty (Zucker, S. et al. 2004), propagating to the RV semi-amplitude K_1 . As shown by Equation 2, the peak K_1 at $i_{\text{initial}} = 75^\circ$ increases linearly from $\sim 530 \text{ m s}^{-1}$ at $m_1 \sin I_1 = 1.8 M_J$ to $\sim 950 \text{ m s}^{-1}$ at $m_1 \sin I_1 = 3.28 M_J$, with the reference value $\sim 750 \text{ m s}^{-1}$ at $m_1 \sin I_1 = 2.54 M_J$. Nonetheless, over 40-year baselines, these amplitude variations induce RV drifts below $0.5 \text{ m s}^{-1} \text{ yr}^{-1}$ superimposed on the underlying vZLK-driven deviations exceeding $\sim 1.9 \text{ m s}^{-1} \text{ yr}^{-1}$ in high-inclination configurations.

Next-generation spectrographs will revolutionize the detection of these dynamical signatures. Instruments like ESPRESSO (Pepe et al. 2013) and the upcoming ANDES/ELT (Marconi et al. 2021) will achieve long-term RV precision of $\sim 10 \text{ cm s}^{-1}$ to 1 m s^{-1} . Combined with astrometric constraints—particularly from

missions like CHES, capable of delivering $\sim 0.1 \text{ AU}$ orbital precision within 100 pc (Feng et al. 2019, 2022; Ji et al. 2022; Huang et al. 2025)—these advances enable refined dynamical modeling and detection of sub- $\text{m s}^{-1} \text{ yr}^{-1}$ secular trends within decadal baselines.

4.2. Impacts of general relativity and tidal effects

In our dynamical modeling, we have exclusively focused on the vZLK driven evolution, deliberately neglecting short-range effects—particularly general relativistic (GR) precession and tidal interactions. These processes can significantly modify or even suppress vZLK oscillations when their characteristic precession rates become comparable to or faster than the vZLK-induced pericenter precession rate (Fabrycky & Tremaine 2007; Liu et al. 2015; Naoz 2016; Lu et al. 2025).

Under the quadrupole approximation, the vZLK-induced pericenter precession rate of the inner orbit is

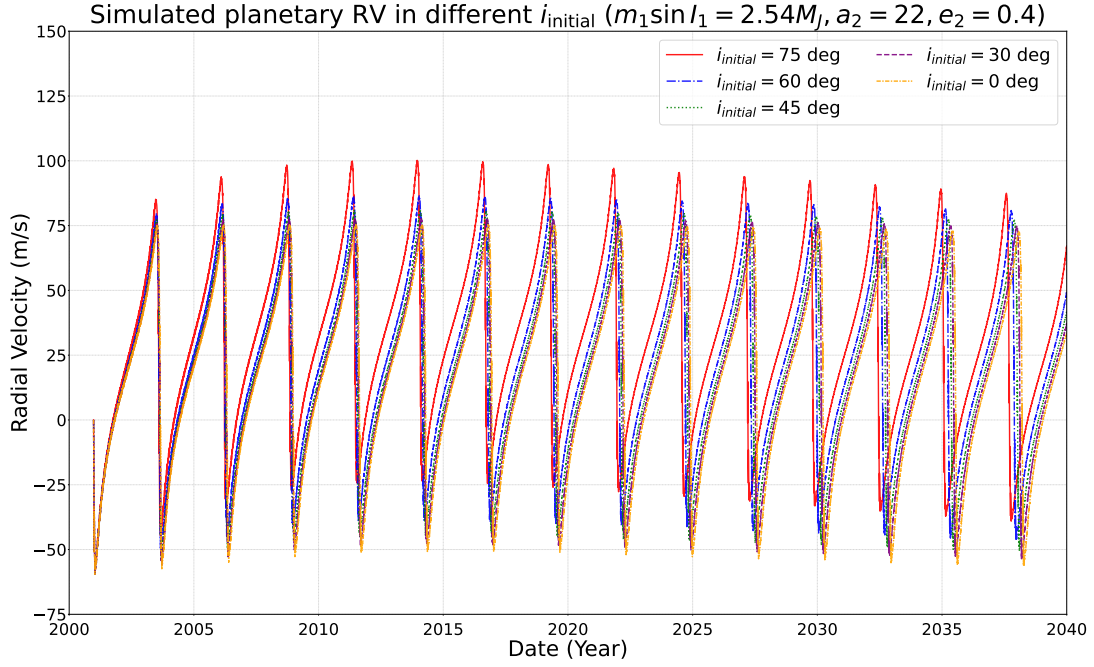
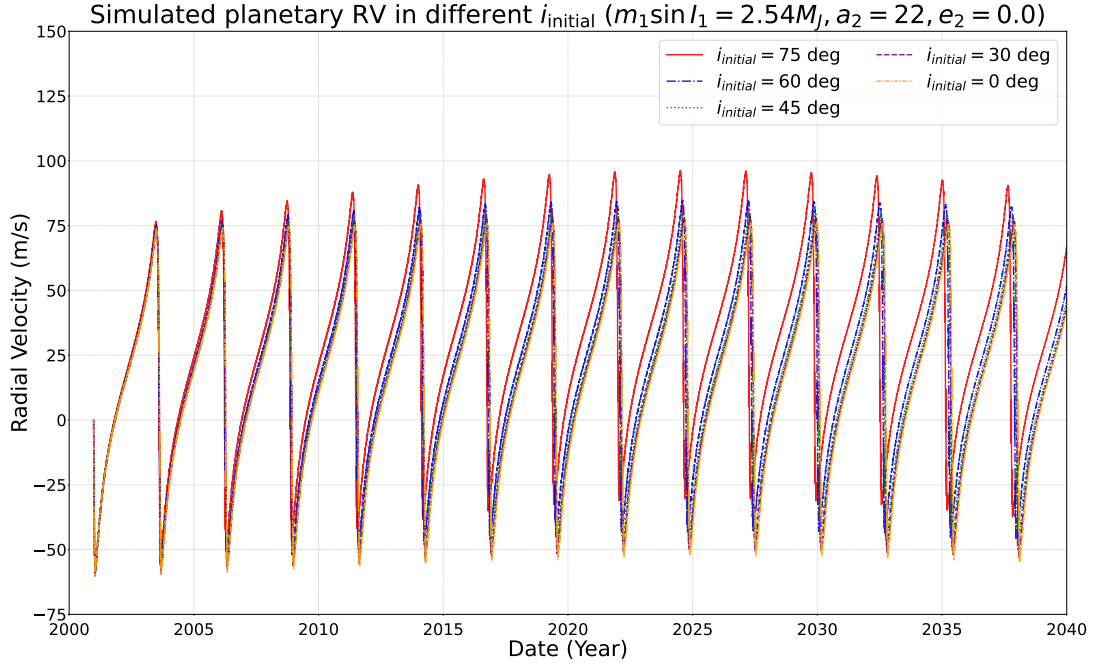


Figure 5. Simulated RV curves of HD 41004 Ab for various initial mutual inclinations (i_{initial}) at $a_2 = 22$ AU and $m_1 \sin I_1 = 2.54 M_J$, with $e_2 = 0$ (top panel) and $e_2 = 0.4$ (bottom panel). The RV signals are plotted over a 40-year baseline, illustrating the influence of different initial mutual inclinations (i_{initial}). In the **top panel**, the configuration with $e_2 = 0$ is shown for i_{initial} ranging from 0° to 75° . The distinct color curves represent varying inclinations, with higher inclinations displaying larger RV amplitudes. The **bottom panel** presents the corresponding configurations for $e_2 = 0.4$, with the same range of initial inclinations.

given by:

$$\begin{aligned} \dot{\omega}_{1,\text{vZLK}} = 6C_2 \left[\frac{1}{G_1} (4 \cos^2 i_{\text{initial}} + (5 \cos 2\omega_1 - 1)) \right. \\ \times (1 - e_1^2 - \cos^2 i_{\text{initial}})) \\ \left. + \frac{\cos i_{\text{initial}}}{G_2} (2 + e_1^2 (3 - 5 \cos 2\omega_1)) \right], \end{aligned} \quad (6)$$

where

$$C_2 = \frac{G^4}{16} \frac{(m_0 + m_1)^7}{(m_0 + m_1 + m_2)^3} \frac{m_2^7}{(m_0 m_1)^3} \frac{L_1^4}{L_2^3 G_2^3}. \quad (7)$$

The pericenter precession rate due to GR is given by (Antoniciello et al. 2021):

$$\dot{\omega}_{1,\text{GR}} = \frac{3G^{3/2}(m_0 + m_1)^{3/2}}{a_1^{5/2} c^2 (1 - e_1^2)}. \quad (8)$$

The pericenter precession rate due to tides is given by (Fabrycky & Tremaine 2007):

$$\begin{aligned} \dot{\omega}_{1,\text{Tide}} = \frac{15\sqrt{G(m_0 + m_1)}}{8a_1^{13/2}} \frac{8 + 12e_1^2 + e_1^4}{(1 - e_1^2)^{9/2}} \\ \times \frac{1}{2} \left[\frac{m_1}{m_0} k_0 R_0^5 + \frac{m_0}{m_1} k_1 R_1^5 \right]. \end{aligned} \quad (9)$$

The parameters k_0 and k_1 are the tidal Love numbers of the star and the planet.

We compute the precession rate ratios $\dot{\omega}_{1,\text{vZLK}}/\dot{\omega}_{1,\text{GR}}$ and $\dot{\omega}_{1,\text{vZLK}}/\dot{\omega}_{1,\text{Tide}}$ for an HD 41004 Ab-like planet across a range of semi-major axes and eccentricities at $m_1 \sin I_1 = 2.54 M_J$. We adopt typical Love numbers of $k_0 = 0.025$ for the primary star and $k_1 = 0.3$ for the planetary companion, representative of solar-type stars and giant planets (Ogilvie 2014). The stellar and planetary radii are set to $R_0 = 0.7 R_\odot$ and $R_1 = 1 R_J$, respectively. The results are shown in Figure 6.

The precession rate ratio $\dot{\omega}_{1,\text{vZLK}}/\dot{\omega}_{1,\text{GR}}$ reaches approximately 3.5×10^5 , while $\dot{\omega}_{1,\text{vZLK}}/\dot{\omega}_{1,\text{Tide}}$ is around 1.8×10^{13} at the nominal system parameters ($a_1 = 1.7$ AU, $e_1 = 0.74$). Taking the simulated vZLK-induced RV drift ($\sim 1.9 \text{ m s}^{-1} \text{ yr}^{-1}$ at $i_{\text{initial}} = 75^\circ$) as a reference, and scaling it using the precession rate ratios and the Keplerian dependence on ω_1 , we estimate 10-year RV variations of only $\sim 5.4 \times 10^{-5} \text{ m s}^{-1}$ for GR and $\sim 1.1 \times 10^{-12} \text{ m s}^{-1}$ for tidal precession. These results indicate that the vZLK mechanism overwhelmingly dominates the precession dynamics. Similar outcomes are found at other inclinations, highlighting that GR and tidal precession are insignificant for HD 41004 Ab at present.

For short-period S-type planets in other compact binaries, e.g. GJ 86 and τ Bootis, short-range forces may

significantly affect the dynamics and should be taken into account to describe their dynamical evolutions accurately.

5. CONCLUSIONS

Through dynamical imprints on observables, secular interactions and mean-motion resonances (MMRs) in multi-planet systems constrain orbital architectures—as demonstrated by Correia et al. (2010) for mutual inclinations, Judkovsky et al. (2022) for long-term trends, and Huang et al. (2025) for MMR-induced RV signatures.

For S-type planets in compact binaries, secular perturbations may be dominated by the vZLK mechanism—replacing MMRs with binary-driven oscillations as the primary dynamical architect. In this study, we investigate the dynamical stability and potential observational signatures of vZLK cycles in the HD 41004 system. Our main conclusions are as follows:

- The planet HD 41004 Ab can remain dynamically stable with mutual inclinations (i_{initial}) up to approximately 75° across various system configurations. The stability analysis has taken into account the fact that the true mass of the planet varies with angle I_1 because of a fixed minimum mass $m_1 \sin I_1$ obtained by RV measurements. Three-body dynamical RV fitting for HD 41004 A across a_2 ranging from 22 to 40 AU and low to moderate e_2 values demonstrates comparable accuracy to Keplerian fits for different i_{initial} . Both stability simulations and RV modeling do not rule out the possibility of a close binary configuration with low or moderate eccentricities. This result highlights that orbits of S-type planets in compact binary systems can maintain stable even under strong secular perturbations.
- Above a critical mutual inclination angle, the vZLK mechanism causes long-term variations in eccentricity, inclination, and apsidal orientation of the planet. With unrestricted three-body simulations, we show that the vZLK timescale shortens significantly with increasing mutual inclination, while the amplitude of inclination oscillations also becomes larger. As a result, highly inclined configurations exhibit stronger and faster RV variations, enhancing the chance of directly observing vZLK effects on accessible timescales. The presence of eccentric vZLK can accelerate these drifts, enhancing the detectability.
- Future RV measurements near periastron could differentiate between high and low mutual inclinations that are both dynamically permitted in this

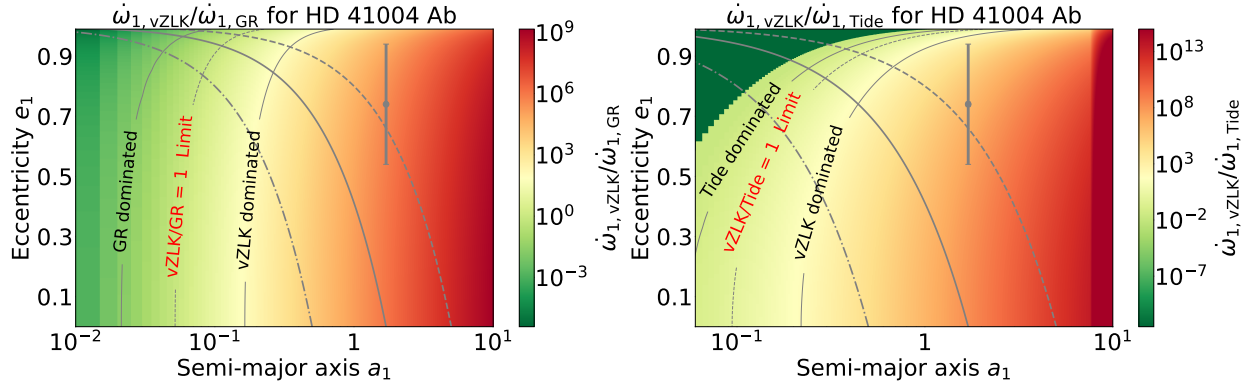


Figure 6. Ratio of vZLK to GR-induced pericenter precession rates ($\dot{\omega}_{1,\text{vZLK}}/\dot{\omega}_{1,\text{GR}}$) and tide-induced pericenter precession rates ($\dot{\omega}_{1,\text{vZLK}}/\dot{\omega}_{1,\text{Tide}}$) for an HD 41004 Ab-like planet as a function of semimajor axis (a_1) and eccentricity (e_1). The color map illustrates the relative dominance of general relativistic and tidal (GR, Tide; green) versus vZLK-induced (red) precession across the (a_1, e_1) parameter space. The gray point with error bars marks the nominal location of HD 41004 Ab, with $a_1 = 1.7$ AU and $e_1 = 0.74 \pm 0.2$. Three gray contours denote the periastron distances typical of warm Jupiters ($a_1 = 0.5$ AU, dash-dotted line), HD 41004 Ab itself (solid line), and cold Jupiters ($a_1 = 5$ AU, dashed line). The system resides well within the vZLK-dominated regime, with a precession rate ratio $\dot{\omega}_{1,\text{vZLK}}/\dot{\omega}_{1,\text{GR}}$ of $\sim 3.5 \times 10^5$ and $\dot{\omega}_{1,\text{vZLK}}/\dot{\omega}_{1,\text{Tide}}$ of $\sim 1.8 \times 10^{13}$ at $i_{\text{initial}} = 75^\circ$.

system. At high inclinations, the effects are particularly pronounced, with RV drifts reaching over ~ 5 m s $^{-1}$ per planetary orbit (~ 1.9 m s $^{-1}$ yr $^{-1}$) at $i_{\text{initial}} = 75^\circ$ and ~ 2.5 m s $^{-1}$ per planetary orbit (~ 0.9 m s $^{-1}$ yr $^{-1}$) at $i_{\text{initial}} = 60^\circ$ in circular binary configuration. In contrast, low-inclination configurations exhibit minimal secular modulation over similar timescales, requiring extended baselines or complementary astrometric data to constrain system parameters. Nonetheless, determining the planet’s true mass can benefit from constraints on the mutual inclination.

Our results suggest that HD 41004 and other similar S-type planetary systems, e.g. GJ 86 (Queloz et al. 2000; Zeng et al. 2022), τ Bootis (Butler et al. 1997; Justesen & Albrecht 2019), GJ 3021 (Naef et al. 2001), HD 196885 (Chauvin et al. 2011, 2023), and HD 164509 (Giguere et al. 2012), are promising targets of studying consequences of secular dynamical effects. Future high-precision RV observations, particularly when combined with astrometric measurements, will enable tighter constraints on the architecture of those hierarchical systems

such as mutual orbital inclination, planetary mass, as well as long-term dynamical evolution.

ACKNOWLEDGEMENT

We thank the referee for many insightful comments that greatly improved the quality of this paper. We also thank Zhecheng Hu, Xiumin Huang, Jianghui Ji, Man Hoi Lee, Doug Lin, Bin Liu, Chris Ormel, Xuesong Wang, and Zixin Zhang for insightful discussions. S.-F.L. acknowledges the support from the Guangdong Basic and Applied Basic Research Foundation under grant No. 2021B1515020090, the National Natural Science Foundation of China under grant No. 11903089, and the China Manned Space Program under grant No. CMS-CSST-2025-A16. B.M. acknowledges the ET2.0 project funding from Shanghai Astronomical Observatory. Z.Q. would like to thank the hospitality of the Proto-planetary Disk and Planet Formation Summer School organized by Xuening Bai and Ruobing Dong in 2022, hosted by the Chinese Center for Advanced Science and Technology.

APPENDIX

A. MEGNO STABILITY ANALYSIS

The Mean Exponential Growth factor of Nearby Orbits (MEGNO) (Cincotta, P. M. & Simó, C. 2000) is a widely used chaos indicator that efficiently distinguishes between stable, quasiperiodic trajectories and chaotic, unstable motion, while also highlighting underlying resonance structures (Maffione et al. 2011). This makes it particularly well-suited for hierarchical three-body systems such as HD 41004, where secular perturbations and strong dynamical coupling can drive complex, long-term orbital evolution.

The MEGNO parameter, $Y(\phi(t))$, quantifies the mean exponential divergence rate between a reference orbit $\phi(t)$ and a nearby orbit $\phi'(t)$ that differs by an infinitesimal perturbation in initial conditions. It is formally defined as:

$$Y(\phi(t)) = \frac{2}{t} \int_0^t \frac{\dot{\delta}(\phi(s))}{\delta(\phi(s))} s ds, \quad (\text{A1})$$

where $\delta(\phi(t))$ represents the time-dependent separation between the two orbits, and $\dot{\delta}(\phi(t))$ is its time derivative. The integrand, $\dot{\delta}/\delta$, corresponds to the instantaneous logarithmic divergence rate, directly related to the maximum Lyapunov Characteristic Exponent (mLCE).

The time-averaged MEGNO value, $\bar{Y}(\phi(t))$, is given by:

$$\bar{Y}(\phi(t)) = \frac{1}{t} \int_0^t Y(\phi(s)) ds. \quad (\text{A2})$$

For stable, quasiperiodic orbits, $\bar{Y}(\phi(t))$ converges asymptotically to 2 as $t \rightarrow \infty$:

$$\bar{Y}(\phi(t)) \simeq 2 - \frac{2 \ln(1 + \lambda t)}{\lambda t} + O(\phi(t)) \rightarrow 2, \quad (\text{A3})$$

where λ is the mLCE. Conversely, for chaotic or unstable orbits, $\bar{Y}(\phi(t))$ diverges from 2 with increasing integration time, clearly signaling dynamical instability.

In the HD 41004 system, instability often manifests through the vZLK-driven excitation of large eccentricities, which may bring the planet's periastron $a_1(1 - e_1)$ close to the stellar Roche limit, leading to tidal disruption or ejection. In our stability assessment, orbits are classified as unstable if the MEGNO value fails to converge to 2 or if the periastron distance falls below the Roche limit during the simulation.

B. DYNAMICAL FITTING OF EXISTING RV DATA FOR DIFFERENT PARAMETERS

Figures 7 and 8 present additional RV modeling of HD 41004 A under different configurations, complementing the analysis in Section 3.2. The structure of these figures follows the same format as Figure 3, with the top, middle, and bottom panels displaying the combined RV signal, the isolated planetary signal, and the O-C residuals, respectively.

Figure 7 investigates the impact of different semi-major axes ($a_2 = 30$ AU and 40 AU) for a fixed minimum planetary mass of $m_1 \sin I_1 = 2.54 M_J$. Figure 8 explores the effect of varying minimum planetary masses ($m_1 \sin I_1 = 1.8 M_J$ and $3.28 M_J$) at $a_2 = 22$ AU. The eccentricities of the stellar companion (e_2) are varied in both cases to assess their influence on the RV curves.

C. TIMESCALE OF VZLK CYCLES

We conduct unrestricted three-body simulations based on the dynamical RV model over a grid of initial mutual inclinations ranging from 0° to 80° , measuring the vZLK timescale for each configuration with year-level precision. For each run, we also record the amplitude of inclination oscillations (i_{\min} to i_{\max}) to quantify the extent of vZLK-induced variations.

Given the uncertainty in e_2 and the instability observed at smaller a_2 for $e_2 = 0.8$, together with the RV fitting results in Section 3.2 that favor low to moderate binary eccentricities, our simulations focus on $e_2 = 0$ and $e_2 = 0.4$ at $a_2 = 22$ AU with $m_1 \sin I_1 = 2.54 M_J$. Although wider a_2 values are still dynamically viable, they exhibit similar secular behavior and are sufficiently captured by analogous cases.

Figure 9 shows the simulation results. In the left panel ($e_2 = 0$), the simulated vZLK timescale systematically decreases with increasing mutual inclination, from $\sim 8.99 \times 10^3$ years at $i_{\text{initial}} = 40^\circ$ to $\sim 2.20 \times 10^3$ years at 80° . The right panel ($e_2 = 0.4$) shows a similar trend, with timescales decreasing from $\sim 4.53 \times 10^3$ years to $\sim 1.70 \times 10^3$ years over the same inclination range. These values remain consistently below the theoretical prediction, also underscore the amplifying effect of binary eccentricity.

The error bars in both panels indicate the oscillation ranges of inclination during the vZLK cycles, with larger spreads at high inclinations. This behavior demonstrates that high-inclination orbits experience both faster vZLK oscillations and larger variations, enhancing the potential for detectable long-term RV signals.

REFERENCES

- | | |
|--|--|
| Andrade-Ines, E., Beaugé, C., Michtchenko, T., & Robutel, | Antognini, J. M. O. 2015, MNRAS, 452, 3610, |
| P. 2016, Celestial Mechanics and Dynamical Astronomy, | doi: 10.1093/mnras/stv1552 |
| 124, 405, doi: 10.1007/s10569-015-9669-5 | |

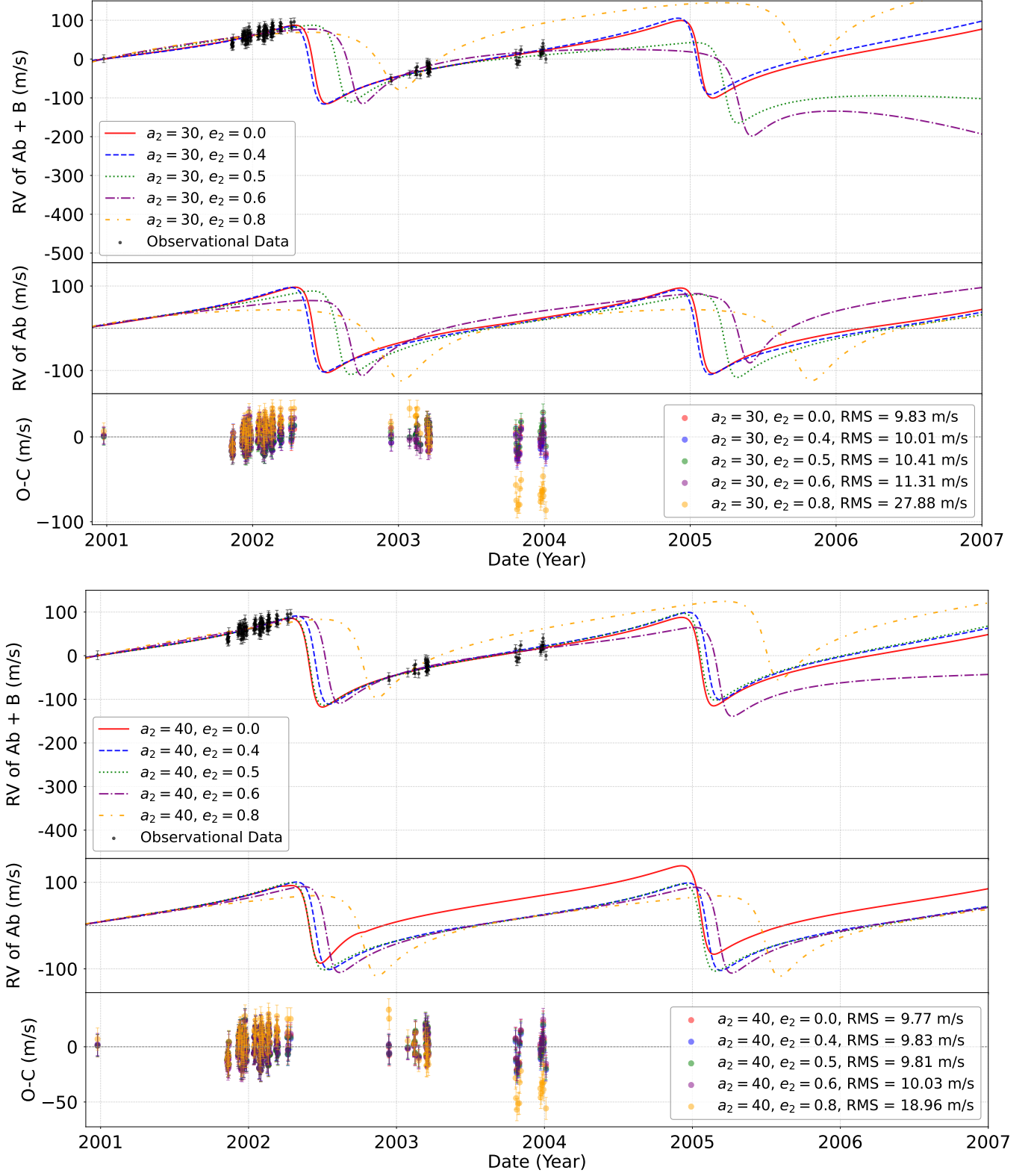


Figure 7. Dynamical RV Fitting of HD 41004 A for $a_2 = 30$ AU and $a_2 = 40$ AU. The structure is the same as Figure 3. Different colors and line styles indicate varying eccentricities. The planetary mass is fixed at $m_1 \sin I_1 = 2.54 M_J$. RMS values of the O-C residuals are listed in the legends.

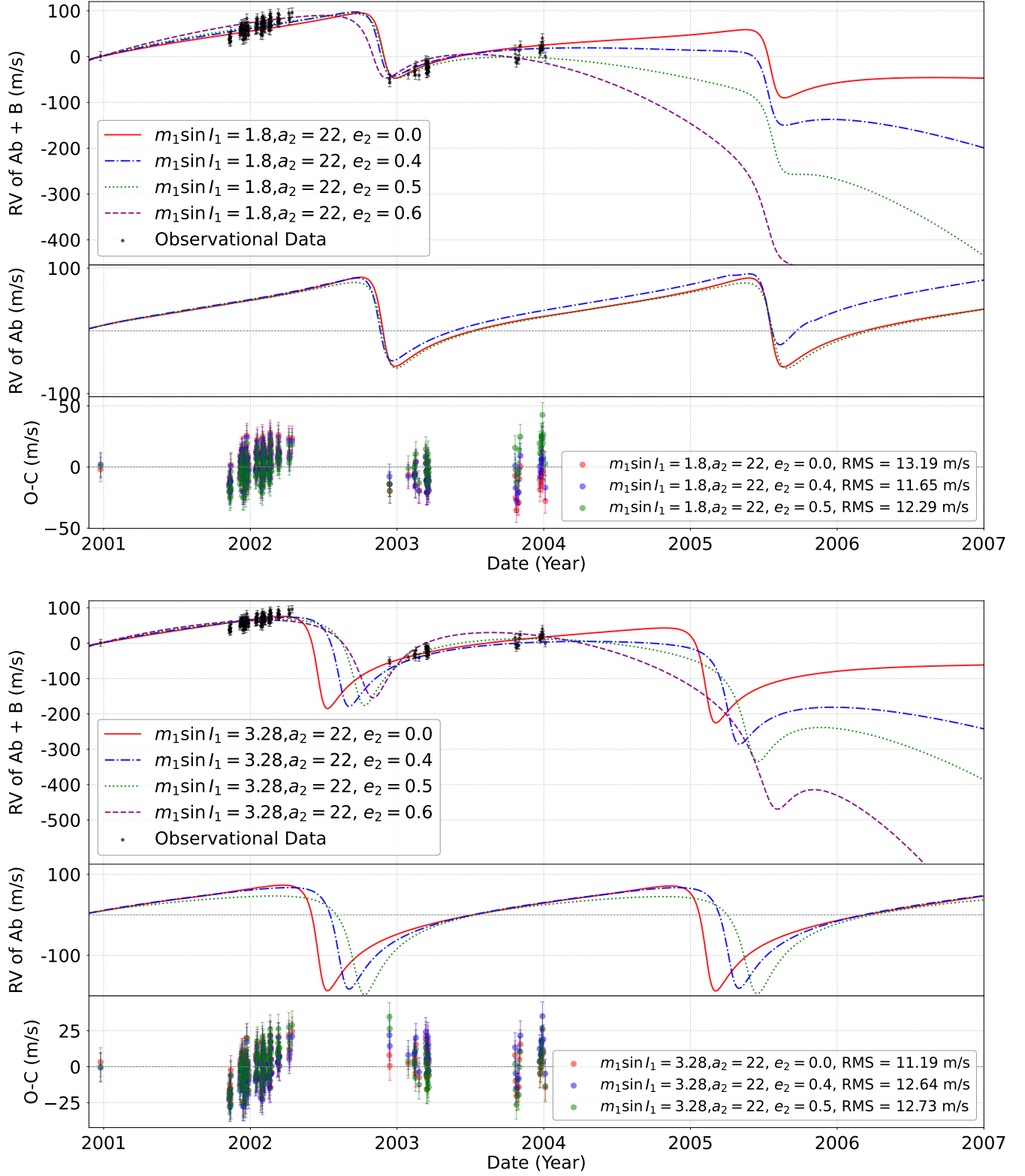


Figure 8. Dynamical RV Fitting of HD 41004 A for different planetary masses at $a_2 = 22$ AU. The structure is the same as Figure 3. The **top panel** represents fits for $m_{\text{pl}} = 1.8 M_J$, while the **bottom panel** corresponds to $m_{\text{pl}} = 3.28 M_J$.

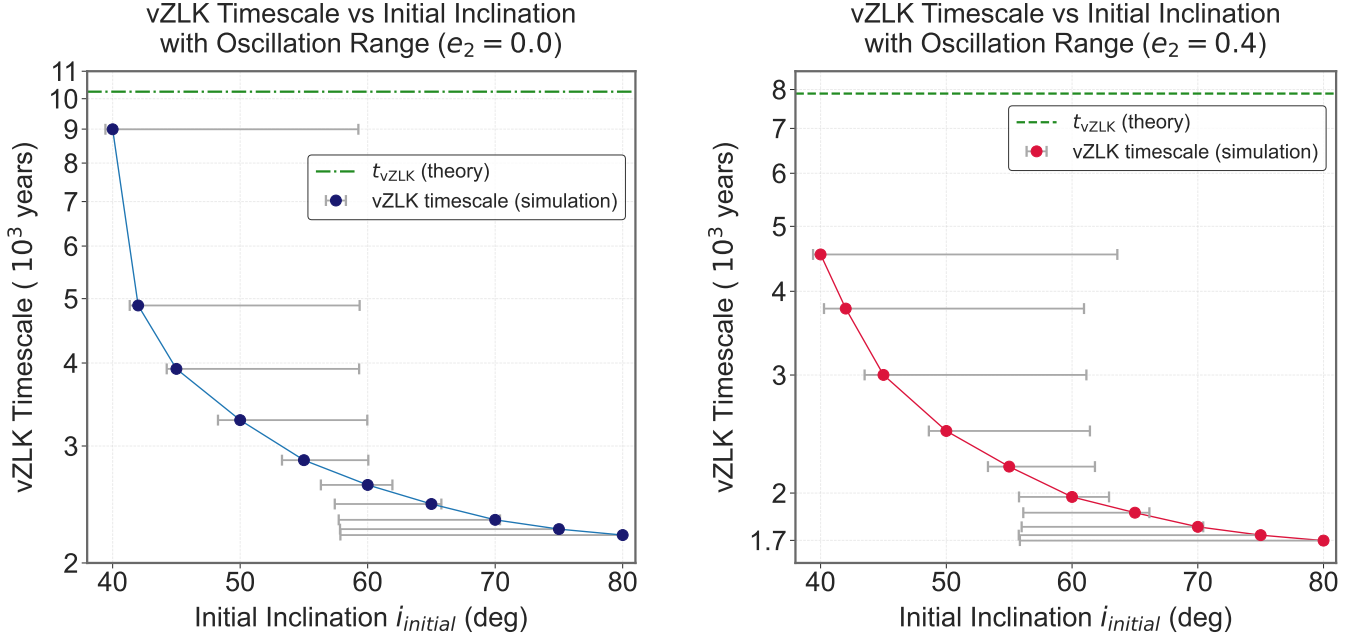


Figure 9. Dependence of the vZLK timescale on the initial mutual inclination in the HD 41004 system for different binary eccentricities. Solid points indicate the simulated vZLK timescales as functions of i_{initial} , with horizontal error bars denoting the corresponding inclination oscillation amplitudes (from i_{min} to i_{max}). The green dash-dotted lines mark the theoretical vZLK timescales derived from the test-particle approximation, calculated as 1.02×10^4 years for $e_2 = 0$ and 7.89×10^3 years for $e_2 = 0.4$. Both panels reveal a systematic decrease in the vZLK timescale with increasing inclination, highlighting enhanced dynamical interactions at higher i_{initial} values.

Antoniciello, G., Borsato, L., Lacedelli, G., et al. 2021, Monthly Notices of the Royal Astronomical Society, 505, 15671574, doi: [10.1093/mnras/stab1336](https://doi.org/10.1093/mnras/stab1336)

Ballantyne, H. A., Espaas, T., Norgrove, B. Z., et al. 2021, Monthly Notices of the Royal Astronomical Society, 507, 4507, doi: [10.1093/mnras/stab2324](https://doi.org/10.1093/mnras/stab2324)

Benettin, G., Galgani, L., Giorgilli, A., & Strelcyn, J.-M. 1980, Meccanica, 15, 9, doi: [10.1007/BF02128236](https://doi.org/10.1007/BF02128236)

Bhaskar, H. G., & Perets, H. 2024, ApJ, 973, 108, doi: [10.3847/1538-4357/ad62f9](https://doi.org/10.3847/1538-4357/ad62f9)

Butler, R. P., Marcy, G. W., Williams, E., Hauser, H., & Shirts, P. 1997, ApJL, 474, L115, doi: [10.1086/310444](https://doi.org/10.1086/310444)

Camargo, B. C. B., Kley, W., & Winter, O. C. 2023, MNRAS, 522, 6394, doi: [10.1093/mnras/stad1455](https://doi.org/10.1093/mnras/stad1455)

Campbell, B., Walker, G. A. H., & Yang, S. 1988, ApJ, 331, 902, doi: [10.1086/166608](https://doi.org/10.1086/166608)

Chauvin, G., Beust, H., Lagrange, A. M., & Eggenberger, A. 2011, A&A, 528, A8, doi: [10.1051/0004-6361/201015433](https://doi.org/10.1051/0004-6361/201015433)

Chauvin, G., Videla, M., Beust, H., et al. 2023, A&A, 675, A114, doi: [10.1051/0004-6361/202244502](https://doi.org/10.1051/0004-6361/202244502)

Cincotta, P. M., & Simó, C. 2000, Astron. Astrophys. Suppl. Ser., 147, 205, doi: [10.1051/aas:2000108](https://doi.org/10.1051/aas:2000108)

Correia, A. C. M., Couetdic, J., Laskar, J., et al. 2010, Astronomy and Astrophysics, 511, A21, doi: [10.1051/0004-6361/200912700](https://doi.org/10.1051/0004-6361/200912700)

Duquennoy, A., & Mayor, M. 1991a, A&A, 248, 485

—. 1991b, A&A, 248, 485

Dvorak, R., Pilat-Lohinger, E., Funk, B., et al. 2002, Astronomy and Astrophysics, 398, <https://api.semanticscholar.org/CorpusID:6311198>

Fabrycky, D., & Tremaine, S. 2007, ApJ, 669, 1298, doi: [10.1086/521702](https://doi.org/10.1086/521702)

Feng, F., Anglada-Escudé, G., Tuomi, M., et al. 2019, Monthly Notices of the Royal Astronomical Society, 490, 50025016, doi: [10.1093/mnras/stz2912](https://doi.org/10.1093/mnras/stz2912)

Feng, F., Butler, R. P., Vogt, S. S., et al. 2022, The Astrophysical Journal Supplement Series, 262, 21, doi: [10.3847/1538-4365/ac7e57](https://doi.org/10.3847/1538-4365/ac7e57)

Ford, E. B., Kozinsky, B., & Rasio, F. A. 2004, The Astrophysical Journal, 605, 966966, doi: [10.1086/382349](https://doi.org/10.1086/382349)

Fragione, G. 2018, Monthly Notices of the Royal Astronomical Society, doi: [10.1093/mnras/sty3367](https://doi.org/10.1093/mnras/sty3367)

Froeschlé, C., Gonczi, R., & Lega, E. 1997, Planetary and Space Science, 45, 881, <https://api.semanticscholar.org/CorpusID:121202999>

Giguere, M. J., Fischer, D. A., Howard, A. W., et al. 2012, ApJ, 744, 4, doi: [10.1088/0004-637X/744/1/4](https://doi.org/10.1088/0004-637X/744/1/4)

Giuppone, C. A., & Correia, A. C. M. 2017, A&A, 605, A124, doi: [10.1051/0004-6361/201730491](https://doi.org/10.1051/0004-6361/201730491)

- Gong, Y.-X., & Ji, J. 2018, *Monthly Notices of the Royal Astronomical Society*, 478, 45654574, doi: [10.1093/mnras/sty1300](https://doi.org/10.1093/mnras/sty1300)
- Greco, J. P., & Burrows, A. 2015, *ApJ*, 808, 172, doi: [10.1088/0004-637X/808/2/172](https://doi.org/10.1088/0004-637X/808/2/172)
- Haghighipour, N. 2006, *The Astrophysical Journal*, 644, 543550, doi: [10.1086/503351](https://doi.org/10.1086/503351)
- Hamers, A. S. 2021, *MNRAS*, 500, 3481, doi: [10.1093/mnras/staa3498](https://doi.org/10.1093/mnras/staa3498)
- Hamers, A. S., & Lai, D. 2017, *MNRAS*, 470, 1657, doi: [10.1093/mnras/stx1319](https://doi.org/10.1093/mnras/stx1319)
- Harrington, R. S. 1968, *AJ*, 73, 190, doi: [10.1086/110614](https://doi.org/10.1086/110614)
- Hatzes, A. P., Cochran, W. D., Endl, M., et al. 2003, *The Astrophysical Journal*, 599, 1383, doi: [10.1086/379281](https://doi.org/10.1086/379281)
- Heintz, W. 1982, *Observatory*, 102
- Heppenheimer, T. A. 1978, *A&A*, 65, 421
- Hill, G. W. 1878, *American Journal of Mathematics*, 1, 5. <http://www.jstor.org/stable/2369430>
- Holman, M. J., & Wiegert, P. A. 1999, *The Astronomical Journal*, 117, 621, doi: [10.1086/300695](https://doi.org/10.1086/300695)
- Huang, X., & Ji, J. 2022, *The Astronomical Journal*, 164, 177, doi: [10.3847/1538-3881/ac8f4c](https://doi.org/10.3847/1538-3881/ac8f4c)
- Huang, X., Ji, J., Bao, C., et al. 2025, *Closeby Habitable Exoplanet Survey (CHES). III. Retrieval of Planetary Masses in Binaries Using the N-body Model with RV and Astrometry Synergy*. <https://arxiv.org/abs/2503.17090>
- Ito, T., & Ohtsuka, K. 2019, *Monographs on Environment, Earth and Planets*, 7, 1, doi: [10.5047/meep.2019.00701.0001](https://doi.org/10.5047/meep.2019.00701.0001)
- Ji, J., Wang, S., Li, H., Fang, L., & Li, D. 2022, *The Innovation*, 3, 100270, doi: [10.1016/j.xinn.2022.100270](https://doi.org/10.1016/j.xinn.2022.100270)
- Judkovsky, Y., Ofir, A., & Aharonson, O. 2022, *The Astronomical Journal*, 163, 90, doi: [10.3847/1538-3881/ac3d95](https://doi.org/10.3847/1538-3881/ac3d95)
- Justesen, A. B., & Albrecht, S. 2019, *A&A*, 625, A59, doi: [10.1051/0004-6361/201834368](https://doi.org/10.1051/0004-6361/201834368)
- Kozai, Y. 1962, *AJ*, 67, 591, doi: [10.1086/108790](https://doi.org/10.1086/108790)
- Laskar, J., & Boué, G. 2010, *A&A*, 522, A60, doi: [10.1051/0004-6361/201014496](https://doi.org/10.1051/0004-6361/201014496)
- Lee, M. H., & Peale, S. J. 2003, *The Astrophysical Journal*, 592, 12011216, doi: [10.1086/375857](https://doi.org/10.1086/375857)
- Li, G., Naoz, S., Holman, M., & Loeb, A. 2014, *The Astrophysical Journal*, 791, 86, doi: [10.1088/0004-637x/791/2/86](https://doi.org/10.1088/0004-637x/791/2/86)
- Lidov, M. 1962, *Planetary and Space Science*, 9, 719, doi: [https://doi.org/https://doi.org/10.1016/0032-0633\(62\)90129-0](https://doi.org/https://doi.org/10.1016/0032-0633(62)90129-0)
- Lithwick, Y., & Naoz, S. 2011, *The Astrophysical Journal*, 742, 94, doi: [10.1088/0004-637X/742/2/94](https://doi.org/10.1088/0004-637X/742/2/94)
- Liu, B., Muñoz, D. J., & Lai, D. 2015, *MNRAS*, 447, 747, doi: [10.1093/mnras/stu2396](https://doi.org/10.1093/mnras/stu2396)
- Lu, T., An, Q., Li, G., et al. 2025, *The Astrophysical Journal*, 979, 218, doi: [10.3847/1538-4357/ad9b79](https://doi.org/10.3847/1538-4357/ad9b79)
- Maffione, N., Giordano, C., & Cincotta, P. 2011, *International Journal of Non-Linear Mechanics*, 46, 23, doi: [10.1016/j.ijnonlinmec.2010.06.008](https://doi.org/10.1016/j.ijnonlinmec.2010.06.008)
- Makó, Z., & Szenkovits, F. 2004, *Celestial Mechanics and Dynamical Astronomy*, 90, 51, doi: [10.1007/s10569-004-5899-7](https://doi.org/10.1007/s10569-004-5899-7)
- Marconi, A., Abreu, M., Adibekyan, V., et al. 2021, *The Messenger*, 182, 27, doi: [10.18727/0722-6691/5219](https://doi.org/10.18727/0722-6691/5219)
- Musielak, Z. E., Cuntz, M., Marshall, E. A., & Stuit, T. D. 2005, *A&A*, 434, 355, doi: [10.1051/0004-6361:20040238](https://doi.org/10.1051/0004-6361:20040238)
- Naef, D., Mayor, M., Pepe, F., et al. 2001, *A&A*, 375, 205, doi: [10.1051/0004-6361:20010841](https://doi.org/10.1051/0004-6361:20010841)
- Naoz, S. 2016, *Annual Review of Astronomy and Astrophysics*, 54, 441, doi: [10.1146/annurev-astro-081915-023315](https://doi.org/10.1146/annurev-astro-081915-023315)
- Naoz, S., Farr, W. M., Lithwick, Y., Rasio, F. A., & Teyssandier, J. 2013, *Monthly Notices of the Royal Astronomical Society*, 431, 2155, doi: [10.1093/mnras/stt302](https://doi.org/10.1093/mnras/stt302)
- Ogilvie, G. I. 2014, *ARA&A*, 52, 171, doi: [10.1146/annurev-astro-081913-035941](https://doi.org/10.1146/annurev-astro-081913-035941)
- Pepe, F., Cristiani, S., Rebolo, R., et al. 2013, *The Messenger*, 153, 6
- Pilat-Lohinger, E., & Dvorak, R. 2002, *Celestial Mechanics and Dynamical Astronomy*, 82, 143, doi: [10.1023/A:1014586308539](https://doi.org/10.1023/A:1014586308539)
- Pilat-Lohinger, E., Funk, B., & Dvorak, R. 2003, *A&A*, 400, 1085, doi: [10.1051/0004-6361:20021811](https://doi.org/10.1051/0004-6361:20021811)
- Pourbaix, D., & Boffin, H. M. J. 2016, *Astronomy&Astrophysics*, 586, A90, doi: [10.1051/0004-6361/201527859](https://doi.org/10.1051/0004-6361/201527859)
- Pourbaix, D., Neuforge-Verheecke, C., & Noels, A. 1999, *A&A*, 344, 172
- Quarles, B., Li, G., Kostov, V., & Haghighipour, N. 2020, *AJ*, 159, 80, doi: [10.3847/1538-3881/ab64fa](https://doi.org/10.3847/1538-3881/ab64fa)
- Quarles, B., & Lissauer, J. J. 2016, *The Astronomical Journal*, 151, 111, doi: [10.3847/0004-6256/151/5/111](https://doi.org/10.3847/0004-6256/151/5/111)
- Queloz, D., Mayor, M., Weber, L., et al. 2000, *A&A*, 354, 99
- Rein, H., & Liu, S. F. 2012, *A&A*, 537, A128, doi: [10.1051/0004-6361/201118085](https://doi.org/10.1051/0004-6361/201118085)
- Rein, H., & Spiegel, D. S. 2015, *MNRAS*, 446, 1424, doi: [10.1093/mnras/stu2164](https://doi.org/10.1093/mnras/stu2164)
- Santos, N. C., Mayor, M., Naef, D., et al. 2002, *Astronomy & Astrophysics*, 392, 215229, doi: [10.1051/0004-6361:20020876](https://doi.org/10.1051/0004-6361:20020876)
- Satyal, S., Hinse, T. C., Quarles, B., & Noyola, J. P. 2014, *MNRAS*, 443, 1310, doi: [10.1093/mnras/stu1221](https://doi.org/10.1093/mnras/stu1221)

- Satyal, S., & Musielak, Z. E. 2016, *Astronomische Nachrichten*, 337, 300, doi: [10.1002/asna.201512305](https://doi.org/10.1002/asna.201512305)
- Satyal, S., Quarles, B., & Hinse, T. C. 2013, *Monthly Notices of the Royal Astronomical Society*, 433, 2215, doi: [10.1093/mnras/stt888](https://doi.org/10.1093/mnras/stt888)
- Stevenson, A. T., Haswell, C. A., Barnes, J. R., Barstow, J. K., & Ross, Z. O. B. 2023, *Monthly Notices of the Royal Astronomical Society*, 523, 189, doi: [10.1093/mnras/stad1441](https://doi.org/10.1093/mnras/stad1441)
- Su, X.-N., Xie, J.-W., Zhou, J.-L., & Thebault, P. 2021, *The Astronomical Journal*, 162, 272, doi: [10.3847/1538-3881/ac2ba3](https://doi.org/10.3847/1538-3881/ac2ba3)
- Szenkovits, F., & Makó, Z. 2008, *Celestial Mechanics and Dynamical Astronomy*, 101, 273, doi: [10.1007/s10569-008-9144-7](https://doi.org/10.1007/s10569-008-9144-7)
- Teyssandier, J., Naoz, S., Lizarraga, I., & Rasio, F. A. 2013, *ApJ*, 779, 166, doi: [10.1088/0004-637X/779/2/166](https://doi.org/10.1088/0004-637X/779/2/166)
- Tory, M., Grishin, E., & Mandel, I. 2022, *PASA*, 39, e062, doi: [10.1017/pasa.2022.57](https://doi.org/10.1017/pasa.2022.57)
- Veras, D., & Armitage, P. J. 2004, *Icarus*, 172, 349, doi: [10.1016/j.icarus.2004.06.012](https://doi.org/10.1016/j.icarus.2004.06.012)
- von Zeipel, H. 1910, *Astronomische Nachrichten*, 183, 345, doi: [10.1002/asna.19091832202](https://doi.org/10.1002/asna.19091832202)
- Wu, Y., & Murray, N. 2003, *The Astrophysical Journal*, 589, 605614, doi: [10.1086/374598](https://doi.org/10.1086/374598)
- Xie, J.-W., Zhou, J.-L., & Ge, J. 2010, *ApJ*, 708, 1566, doi: [10.1088/0004-637X/708/2/1566](https://doi.org/10.1088/0004-637X/708/2/1566)
- Zeng, Y., Brandt, T. D., Li, G., et al. 2022, *AJ*, 164, 188, doi: [10.3847/1538-3881/ac8ff7](https://doi.org/10.3847/1538-3881/ac8ff7)
- Zucker, S., & Mazeh, T. 1994, *ApJ*, 420, 806, doi: [10.1086/173605](https://doi.org/10.1086/173605)
- Zucker, S., & Mazeh, T. 2002, *The Astrophysical Journal*, 568, L113, doi: [10.1086/340373](https://doi.org/10.1086/340373)
- Zucker, S., Mazeh, T., Santos, N. C., Udry, S., & Mayor, M. 2003, *A&A*, 404, 775, doi: [10.1051/0004-6361:20030499](https://doi.org/10.1051/0004-6361:20030499)
- . 2004, *A&A*, 426, 695, doi: [10.1051/0004-6361:20040384](https://doi.org/10.1051/0004-6361:20040384)